Ann. Geophysicae 11, 797–808 (1993)

Annales Geophysicae

Mesospheric observations with the EISCAT UHF radar during polar cap absorption events: 2. Spectral measurements

M.T. Rietveld [1], **P.N. Collis** [2]

[1] EISCAT Scientific Association, N-9027 Ramfjordbotn, Norway
[2] EISCAT Scientific Association, Box 812, S-981 28 Kiruna, Sweden

Received August 12, 1992; revised April 1, accepted April 5, 1993

Abstract. Incoherent scatter radar spectral measurements of the ionospheric D-region made by the EISCAT UHF (933 MHz) radar between altitudes of 55 and 82 km during polar cap absorption conditions in 1989 and 1990 are presented and analysed. The analysis technique is described and the average Doppler shift of the spectral fits is interpreted in terms of meridional neutral winds. The spectral widths above 70 km are found to be narrower than those expected based on the CIRA-86 atmospheric model and a simple molecular ion gas with average mass of 31 amu, confirming previous work. Below this altitude the broadening of spectral width is interpreted as being caused by the presence of negative ions. The resulting values of negative ion number density to electron number density are approximately consistent with those measured by rockets when allowances are made for the differences in solar zenith angle. A new result is the deduced variation of this ratio through sunset.

Introduction

Spectral measurements in the ionospheric D-region are generally difficult to make with the incoherent scatter radar (ISR) technique. The undisturbed D-region has negligible ionisation at night and is only very weakly ionised by day. Typical daytime electron densities are of the order of 10^8 m^{-3} at 80 km. At this height and below, integration times of the order of tens of minutes are needed to obtain useful spectra with the Arecibo incoherent scatter radar (e.g. Mathews, 1984; Fukuyama *et al.*, 1987). At high latitudes, the precipitation of charged particles radically modifies the electron density profile. Electrons of sufficient energy (tens or even hundreds of keV) can penetrate the mesosphere, causing excess ionisation there. Such events are usually quite brief, however, and regular observations by the EISCAT radar have shown that it is rare for electron precipitation to reach 70 km altitude.

Correspondence to: M. T. Rietveld

Energetic proton precipitation (several tens of MeV), on the other hand, in association with solar proton events, does cause excess ionisation deep into the mesosphere. This increased ionisation, which is particulary concentrated around the polar cap, causes increased absorption of HF radio waves, termed a polar cap absorption (PCA) event. Enhanced electron densities at heights down to about 50 km are not unusual during such conditions (e.g. Reagan and Watt, 1976). Hence, during PCAs, the ionosphere offers a sizeable target to an ISR at altitudes not usually accessible to the technique. The scattered power returned to the radar can be used to determine the ionospheric electron concentration: sample profiles from EISCAT UHF radar observations during some of the events discussed below are given by Collis and Rietveld (1990), which forms a companion study to the present paper. Our objective here is to present the results of EISCAT measurements of incoherent scatter spectra during PCA events.

Röttger and Meyer (1987) have deduced mesospheric wind velocities from the second moment of the UHF spectrum measured using a multi-pulse modulation in the interval 80–105 km; in one case results were obtained down to about 70 km. Spectral measurements have also been made by the EISCAT UHF radar during the PCA event covering 12–15 August 1989 at alitudes of 70–90 km by Hansen *et al.* (1991), who used the same measuring algorithm as that employed for our observations. The present data are the first reported spectral measurements from altitudes below 70 km from the EISCAT UHF radar. Observations were obtained from as low as 55 km in some cases. Particular emphasis is placed on the analysis technique, the altitude variations of the width of the spectra, and on the motions of the neutral atmosphere deduced from the Doppler shifts of the spectra.

Experimental technique

The relatively large neutral gas density in the mesosphere dictates that a different ISR experimental tech-

nique to that used for observations from higher altitudes has to be applied. This arises because the thermal motions of the ions in the D-region are severely modified by their collisions with neutral gas molecules. Hence, the spectral width of the ion line measured by the incoherent scatter technique decreases rapidly with decreasing altitude in the D-region, from about 1 kHz at 90 km to a few tens of Hz at 70 km, for observations at the EISCAT UHF frequency of 933 MHz (Collis and Röttger, 1990). These values will vary somewhat depending on the properties of the neutral and ionised atmospheric gas (see below), but are to be contrasted with typical E-region spectral widths of several kHz, and 10–20 kHz in the F-region (again, at 933 MHz). Spectra from the latter two regimes can be resolved with appropriate height resolution by the multi-pulse, and single-pulse correlation techniques, respectively. The much narrower mesospheric spectra (corresponding to longer correlation times), however, require a longer lag increment for the computation of the autocorrelation function (ACF) of the scattered signal. This is achieved with the so-called pulse-to-pulse correlation technique, in which the scattered signal is sampled after each of a train of pulses, separated by typically 1–5 ms, which defines the lag increment of the ACF (Kofman, 1982; Mathews, 1986).

Accurate determination of the weak, narrow signal of the mesospheric incoherent scatter spectrum depends on how successfully unwanted noise can be excluded from the measurements. Under normal circumstances the signal is very much weaker than the noise. One component of this noise is intrinsic to the nature of the scattering itself and can only be reduced by averaging many samples. Other sources of noise can include ground clutter, ionospheric clutter from preceding pulses, instrument noise (including mains contamination) and gain variations. Post-processing of the data (or real-time analysis if sufficient computing power is available) can be used to reject some additive noise which exceeds statistically expected values (German and Mathews, 1986; Ying *et al.*, 1987).

Some degree of noise elimination can also be achieved by including compensating features in the experiment design. Such is the case with the pulse-to-pulse correlation algorithm used for the radar operations described below, termed GEN-11 (Turunen, 1986). The basic components of this pulse scheme are double 13-bit Barker codes with bit length 7 μs, yielding a range resolution of 1050 m. The second of the double pulses has inverted phase and the separation between the double pulses is varied successively for five pairs, after which the cycle repeats. These features allow suppression of most of the unwanted noise. However, this design also introduces range ambiguities, and lag-dependent clutter to the measured ACF. Contamination at lag numbers divisible by five is particularly severe due to the modulo 5 repetition of the transmission pattern. Removal of the effects of range ambiguity can be accomplished by applying corrections based on the theory of ambiguity functions (Pollari *et al.*, 1989). Such corrections were made when analysing the data from the GEN-11 experiments described below, but the lag-dependent clutter which often existed in the first five gates was not accounted for. Hence, the sixth range-gate usually defined the lowest altitude from which reliable results could be obtained: this was at 55 km altitude when the antenna was lowered to 45° elevation (see below). The highest of the 42 signal gates with this geometry is at 80 km altitude. The lag separation of 2.222 ms in the correlation estimates dictates a maximum bandwidth of the received signals of ±225 Hz. This effectively excludes reliable spectral measurements above about 85 km altitude.

GEN-11 was originally designed for the EISCAT VHF (224 MHz) radar, so the frequency bandwidth is often too small at UHF (933 MHz) frequencies. Useful measurements have, however, been made at UHF in the height range 75–90 km during periods of auroral electron precipitation (e.g. Turunen *et al.*, 1988). The present measurements were obtained under the more unusual conditions of PCA events. Table 2 of Collis and Rietveld (1990) lists such events for 1989. Of those listed and during which the GEN-11 experiment was run, only the events of 20 October, 23 October and 1 December provided useful spectra well below 70 km. In addition to these, we use data from a later PCA event on 20 March 1990. For purposes of comparison we also make use of further results from above 75 km from other GEN-11 operations during non-PCA conditions (6 May and 2 July 1988). The duration of these experiments varied from about 2 to 5 h, although sometimes other experiments were run during other parts of the PCAs. Examples of electron density profiles from some of the GEN-11 experiments during PCA events which will be examined here are shown in Figs. 6–9 of Collis and Rietveld (1990).

Analysis procedure

Initial development of the theory of incoherent scattering from a collision-dominated plasma was presented by Dougherty and Farley (1963). Later refinements have also considered the effect of negative ions and different positive ion masses (Mathews, 1978; Fukuyama and Kofman, 1980) and the effect of chemical fluctuations (Wisemberg and Kockarts, 1983). Present consensus indicates that the spectral shape in the mesosphere can be approximated by a Lorentzian distribution (Mathews, 1986):

$$S(f)=A_1/(1+((f-A_3)/A_2)^2)+A_4\,, \qquad (1)$$

where A_1 is the maximum amplitude of the spectrum, A_2 is the full width of the spectrum at half-maximum amplitude (called spectral width), A_3 is the Doppler shift from zero frequency and A_4 is a base value representing background noise and folded-in electron line contributions, as illustrated in Fig. 1. In terms of geophysical parameters, the total power under the spectrum yields electron concentration (with modifications if negative ions are present) and the Doppler shift converts to line-of-sight ion velocity. The very large ion-neutral collision frequencies at these altitudes result in the bulk ion motions following those of the neutral atmosphere. Hence, the Doppler shift simply yields the line-of-sight component of the neutral wind. The spectral width is a more involved quantity and contains contributions from four main parameters, the individual effects of which cannot be unambiguously de-

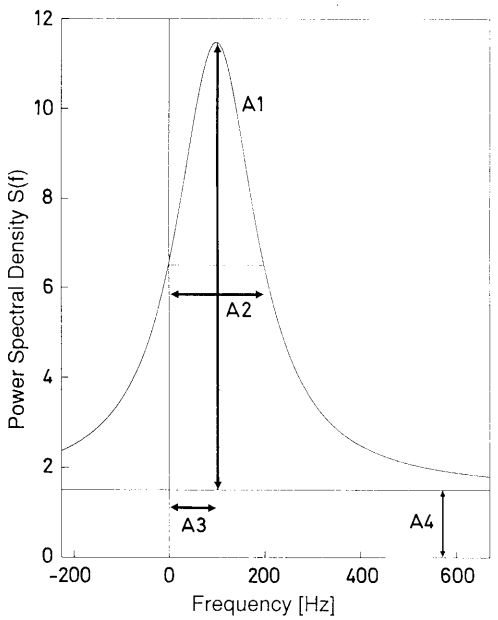

Fig. 1. The parameters defining an incoherent scatter spectrum of Lorentzian shape. The parameters are defined by Eq. (1). $S(f)$, the power spectral density, is in arbitrary units

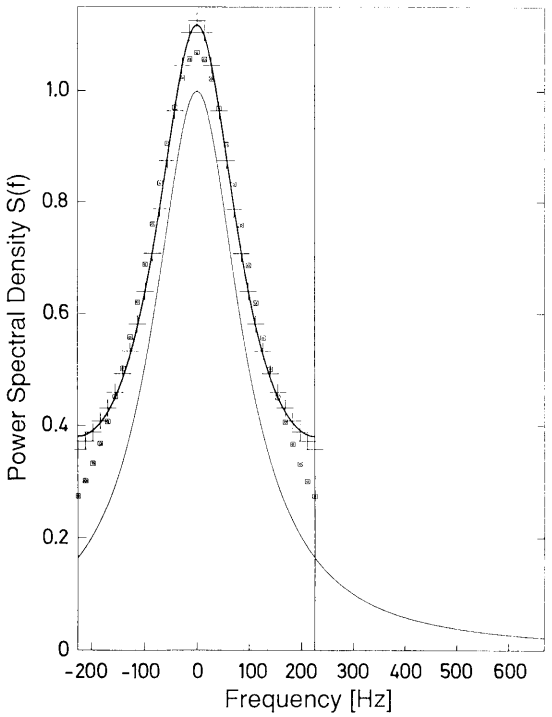

Fig. 2. Example of the effects of aliasing on a broad Lorentzian spectrum. The *thin solid line* shows the original spectrum and the *thick solid line* the aliased spectrum. Analytical fits to the aliased spectrum using three parameters (*squares*) and four parameters (*crosses*) are also shown

convolved from a single spectrum. In order to obtain quantitative geophysical information from the spectral width, it is necessary to make assumptions (for example, to use models) or to have independent measurements of one or more of the parameters involved. The simplest functional form of the spectral width, W, neglecting finite Debye length effects, is

$$W = C(1+\lambda)\, T/\nu_{\text{in}}\, m_i\,, \tag{2}$$

where λ is the ratio of negative ion number density to electron number density, T is the neutral temperature, ν_{in} is the ion-neutral collision frequency and m_i is the mean mass of positive ions. C is a constant equivalent to $32\pi k_B/\lambda_R^2$ (e.g. Mathews, 1978) where k_B is Boltzmann's constant and λ_R is the radar wavelength. If the effect of finite Debye length, λ_D, is to be included, Eq. (2) becomes

$$W = C\,T((1+\lambda)+\alpha^2/2)/\nu_{\text{in}}\, m_i\,(1+\alpha^2)\,, \tag{3}$$

where

$\alpha = 4\pi\lambda_D/\lambda_R$ and λ_D is given by $\lambda_D = \sqrt{(\varepsilon_0\, k_B\, T)/(N_e\, e^2)}$ where ε_0 is the permittivity in a vacuum, N_e is the electron density and e the electronic charge.

The spectral width of a Lorentzian curve at half-maximum amplitude, W, is related to correlation time, T_c, of the exponential ACF by

$$W = 1/(\pi\, T_c)\,. \tag{4}$$

ACFs of the backscattered signals are recorded in the EISCAT data recording system. In the analysis one can either fit ACFs directly to the data, as done by Hoppe and Hansen (1988) and Hansen *et al.*, (1991), or a Lorentzian function given by Eq. (1) can be fitted to the spectrum calculated from the measured ACF. In our analysis we have tried both methods and the results are compared below.

Spectral fitting

The analysis of the spectra consisted of integrating the data for typically 2 or 5 min; correcting the ACF for range side-lobes of the Barker code using a method based on that of Polarri *et al.* (1989); calculating the spectrum; and least-squares fitting the constants which define the spectral shape of the ion line. When the intrinsic spectral width is large there may be aliasing of the wings of the Lorentzian spectrum which lie outside ± 225 Hz, as is illustrated schematically in Fig. 2. The thick solid line shows the spectrum measured by the GEN-11 experiment for an intrinsic spectrum shown by the thin solid line. The filter width is ± 70.7 kHz, but the requirement of coherence over the timescale of 91 μs (13-pulse Barker code with 7 μs baud) in order for the Barker coding to work means that any remaining signal outside ± 5.5 kHz will be reduced by 1/13 in a given range gate.

To determine the effect of aliasing on the fitting of broad Lorentzian spectra, we generated a spectrum with a given width and repeatedly folded in the power falling outside ± 225 Hz to simulate our measured spectra. We then fitted a four-parameter Lorentzian of the form given by Eq. (1), shown by the crosses in Fig. 2. A three-parameter fit with the term A_4 set to zero is shown by the squares, clearly indicating that the four-parameter fit is the correct one to use. The fitted value of A_2 was 180 Hz for an intrinsic width of 200 Hz, which illustrates that the effect of aliasing of the broad spectra is to cause an underestimation of the spectral width when the fitting is done

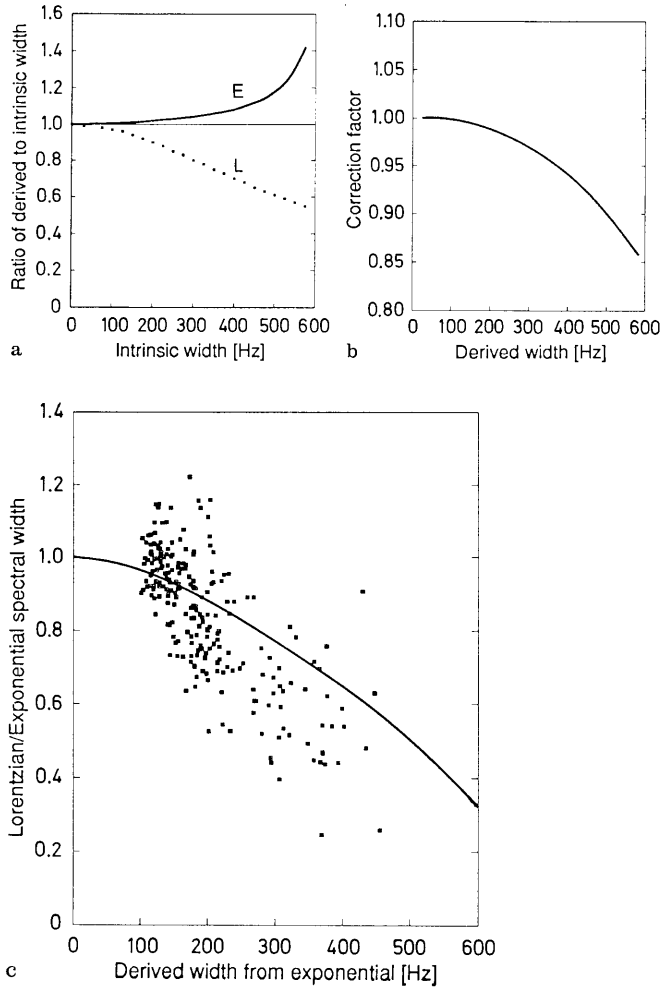

Fig. 3a–c. Results from analytical fitting to simulated spectra. **a** The ratio of derived spectral width to actual width from two approaches using an exponential fit (*E*) to the ACF and a Lorentzian fit (*L*) to the spectrum. **b** The resulting correction factor which needs to be applied to widths derived from the exponential fit. **c** A comparison of the ratio of widths deduced from the two methods applied to actual data (*points*) with the ratios expected from the simulations (*line*)

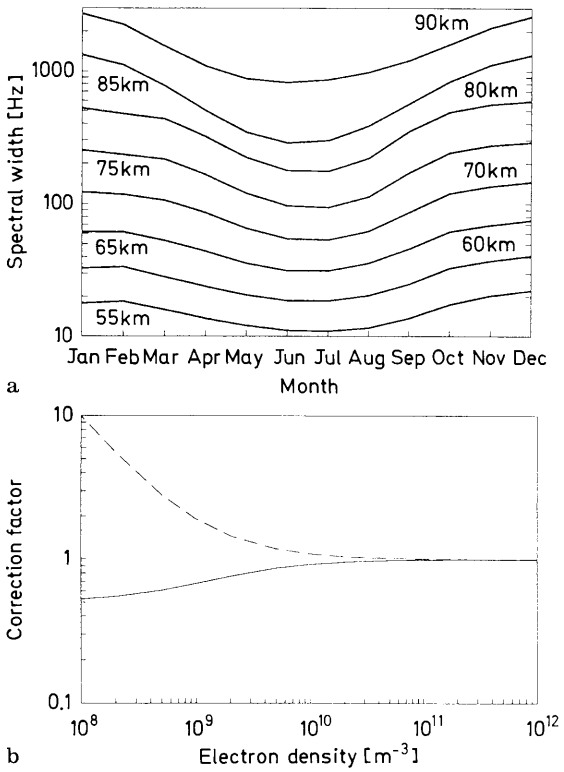

Fig. 4. a Calculated spectral width at 933 MHz as a function of month and altitude, obtained using Eq. (2) and atmospheric parameters from the CIRA-86 model. **b** Corrections to be applied to calculated spectral widths (*solid line*) and to derived λ values (*dashed line*) using Eq. (2) to allow for finite Debye length

in the frequency domain. The other parameters such as Doppler shift and total power are not affected.

The alternative approach to estimating spectral width – that of fitting an exponential to the absolute magnitude of the ACF – was simulated by calculating the ACF of the aliased spectrum (with zero Doppler shift), and fitting an exponential. The spectral width, obtained from the correlation time by using Eq. (4), was 202 Hz, which is much closer to the intrinsic width than that found from the fit in the frequency domain. Figure 3a shows how the ratio of the derived spectral width to the intrinsic width varies as a function of intrinsic width for the two different approaches. It is evident that fitting an exponential to the ACF gives a better estimate of the spectral width, especially above about 100 Hz. Figure 3b shows the correction factor one should use for calculating the spectral width from exponential ACF fitting as a function of the derived (overestimated) width.

Since we do not know the intrinsic width of the measured spectra, it is difficult to know how valid the above simulations are when applied to actual measurements. The check whether the measured data give results consistent with the simulations, we have plotted in Fig. 3c the ratio of spectral widths obtained by the two approaches as a function of width obtained by the ACF method for spectra measured near 1330 UT on 23 October 1989. The dots show the results of fitting to the data while the solid line shows the prediction from the simulated data. The measured results show considerable spread because of the noise contribution to the real spectra, but nevertheless the trend is consistent with that expected from the simulations. The Lorentzian fit is even worse than 'expected' for spectra wider than 225 Hz, indicating that the experimental bandwidth dictates how successful this approach can be.

In the following analysis we shall use velocities and total power derived from the four-parameter Lorentzian fit, and the spectral width from the two-parameter exponential fit.

To give an idea of the expected variation of spectral width with height and season, we calculated the widths for $\lambda = 0$ and $\alpha = 0$, with a positive ion mass of 31 amu (for a 50% NO^+ and 50% O_2^+ ion composition) and ν_{in} calculated according to Hill and Bowhill (1977). The values of ν_{in} depend on temperature and neutral mass density, both of which were obtained from the CIRA-86 model for

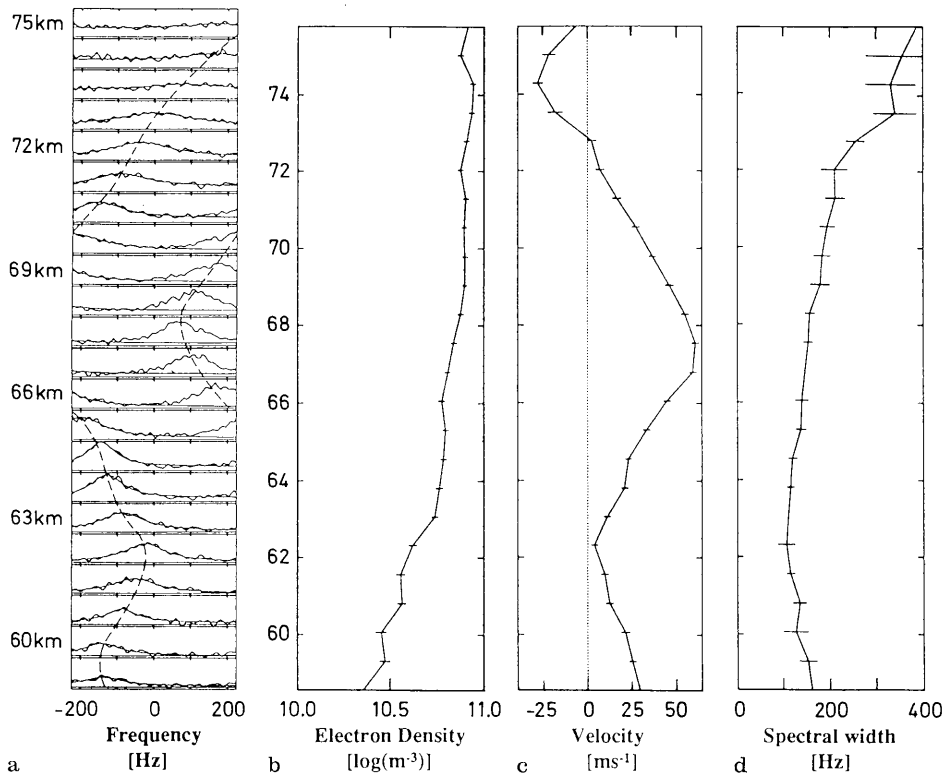

Fig. 5. **a** Profiles of spectra (1 Dec 89, 1112 UT) showing aliasing caused by large velocities. Derived parameters together with their *error bars* are shown to the right. **b** The derived electron density, **c** line-of-sight velocity and **d** spectral width derived from the exponential fit to the ACF.

70°N (Rees, 1990). The results in Fig. 4a show that the width is expected to vary by about a factor of two during the year for a given height, and that it varies by over two orders of magnitude in the altitude range 55–90 km.

The effects of finite Debye length on the spectral width and on derived values of λ are shown in Fig. 4b. The solid line shows the ratio of the spectral width calculated from Eq. 2 to that from Eq. 3. The broken line then shows the factor by which negative ion ratios derived using Eq. (2) need to be multiplied if Debye length effects are correctly accounted for. In our data the densities during the PCAs are almost always larger than 10^{10} m^{-3}, so these factors amount to a contribution of about 10% at most for the cases studied.

Aliasing of velocities

As an example of the data available for this study, Fig. 5a displays stacked spectra illustrating the main features of spectral width and Doppler shift variations with height. In this example, the UHF antenna was pointed at 45° elevation to the north, allowing spectral measurements down to 55 km. The integration time used was 2 min. When the spectra are Doppler-shifted by more than ± 225 Hz, as is the case here because of the large horizontal wind components at some altitudes, aliasing of the line-of-sight Doppler shifts will also occur. In our analysis this is taken into account by assuming continuity of the Doppler shifts between adjacent 1.05-km range gates, and assuming that there exists a height where the spectra are not aliased. This procedure can usually be verified by observing how the Doppler shifts change as the antenna is moved away from vertical where the velocities are small. An example of Doppler aliasing is shown in the left panel of Fig. 5, where the dashed line shows the derived Doppler shifts. The other panels in Fig. 5 show profiles of the electron density, spectral width, and the line-of-sight Doppler velocity, together with their errors derived from the spectra at the left.

Meridional neutral winds

In Fig. 6, we display profiles of the horizontal winds derived from data such as those in the left panel of Fig. 5, for the four GEN-11 experiments during PCAs in 1989/1990. To obtain the horizontal velocities, we assume that the vertical velocities are zero. Because the antenna is directed due north, the meridional component of the neutral wind is measured. The lower boundary of the velocity data is determined in some cases by the low signal-to-noise ratio when the electron density decreases at sunset (e.g. 23 October), and in others by the antenna being at too high an elevation to sample the lowest heights (e.g. 1 December).

During most of the events there is a background northward wind with a superimposed wave-like velocity structure. In three of the four events there is a pronounced peak in velocity of 50–80 m s^{-1} at around 70 km. In the plots for 23 October and 1 December, we have marked descending peaks in the velocities with solid lines. The slopes range from -0.85 to -1.0 km h^{-1} and in the 23 October case it appears as if there is a wave with a vertical wavelength of about 10 km. Using 10 km and 0.85 km h^{-1} for the 23 October data, the wave period would be

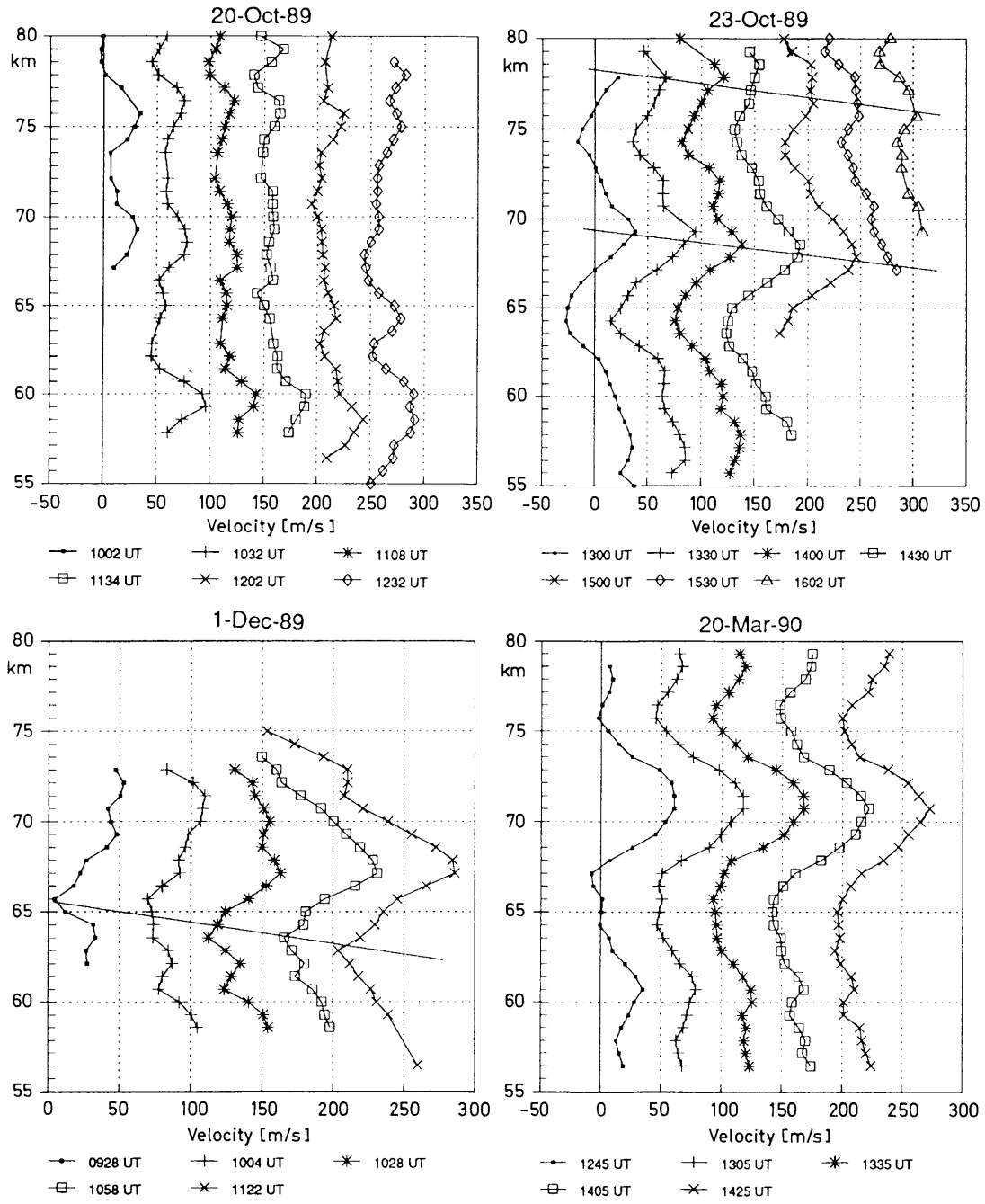

Fig. 6. Sequences of northward wind velocity profiles separated by approximately 30 min for 2-min integrated data on four different days during PCA conditions. Each profile is successively offset by 50 m s^{-1} to the right. The *sloping straight lines* indicate downward propagating velocity structures

12 h, a semi-diurnal tide. This finding would complement the earlier measurements by Röttger and Meyer (1987) of semi-diurnal tides in the 80–105 km range found using EISCAT UHF data. They found that below 80 km the meridional as well as the zonal component of the semi-diurnal tide was approximately 5 m s^{-1}. Taking reasonable errors in our derived values, however, the period could lie in the range 9–14 h which would encompass a 10-h period which has also been measured at Andøya, near Tromsø, by Rüster *et al.* (1988) using the SOUSY VHF radar. At mid-latitudes similar vertical wavelengths of 5–15 km with a mean of 9.5 km in the height range 60–90 km with periods between 8 and 11 h and a mean of 8.6 h have been measured by the MU radar in Japan (Tsuda *et al.*, 1990). The dominant gravity waves were found to have a downward phase progression of -1.12 km h^{-1}, similar to the value deduced above.

The rate of phase progression for the 1 December event is -1.6 km h^{-1}, which, with a vertical wavelength estimate of at least 10 km, results in a period for the wave

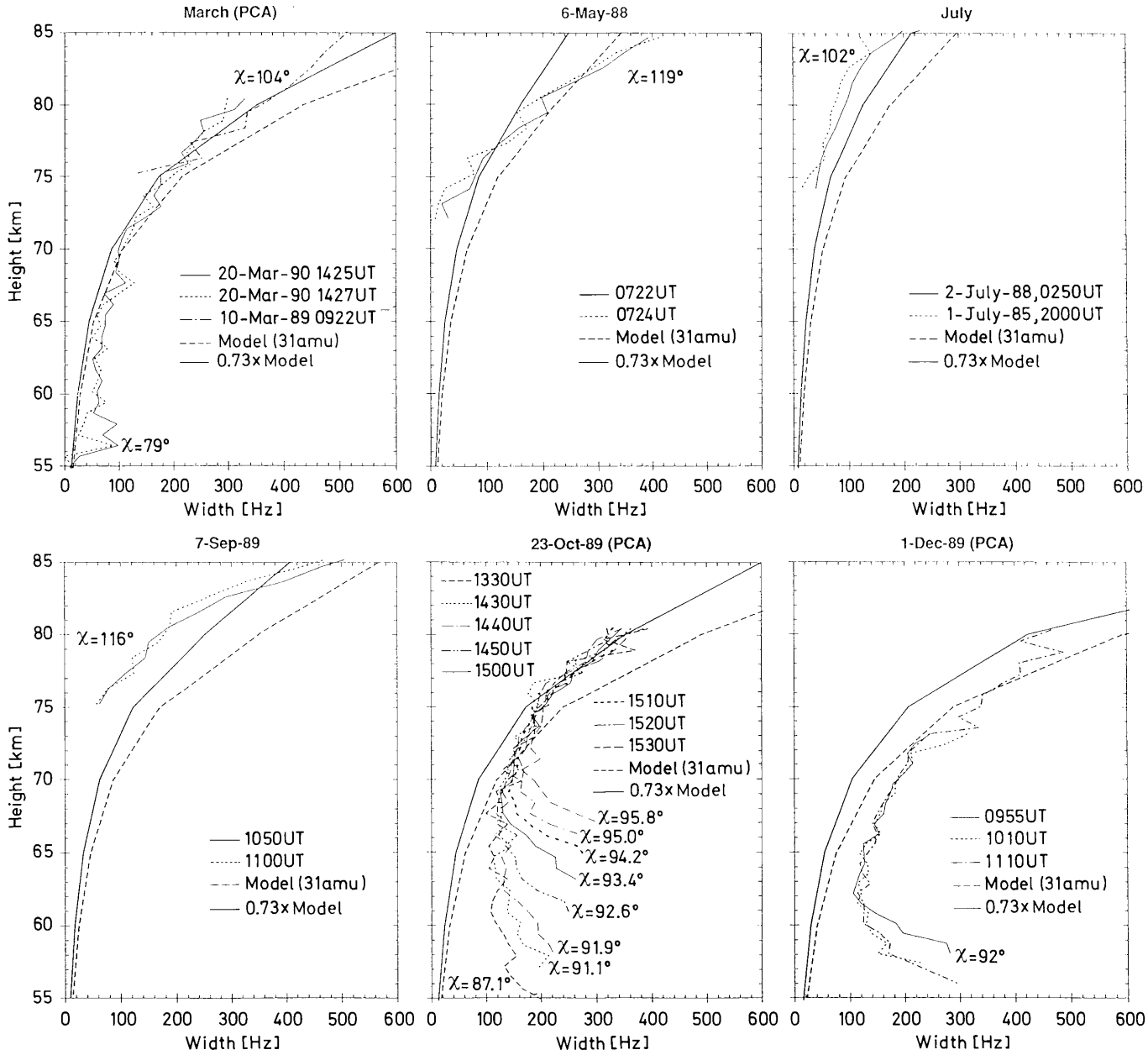

Fig. 7. Measured spectral width profiles during conditions of PCA (Mar, Oct, Dec) and auroral disturbance (May, Jul, Sep). The model widths (*dashed lines*) using 31 amu are also shown in Fig. 4. The *solid lines* show 0.73 times these widths, corresponding to the limit of infinite positive ion mass. The experimental values are labelled with the solar zenith angles (χ) at the times of the measurements

of at least 6 h. Balsey *et al.* (1983) found waves with an 8-h period in VHF data from Poker Flat, Alaska, as did Rüster *et al.* (1988) at Andøya.

Without properly identifiying and removing the long period gravity waves or tides it is difficult to estimate the mean (meridional) wind from our data. It was either close to zero (23 October) or positive (northward) and about 20–30 m s^{-1} for the other events. A northward-directed wind in March and October is consistent with average northward winds ranging from 6 to 11 m s^{-1} measured at Poker flat at heights of 75–80 km for these months (Rees, 1990).

The largest northward velocities, of about 80 m s^{-1}, were observed on 1 December 1989, corresponding to the data shown in Fig. 5. Whether the velocity structures in Fig. 6 are typical of these latitudes or are a result of the PCA events is not easy to determine since we cannot normally measure velocities at these heights.

Clearly, longer time series are required to resolve waves of such long periods. Because of the dependence of the signal strength on the solar zenith angle, however, it will be difficult to get a long uninterrupted time series of velocity data, unless measurements can be obtained during a PCA within a few weeks of midsummer. Because the signals are relatively strong as well as only slowly varying under PCA conditions, the integration time required to derive the spectral parameters is short (of the order of a minute), so that one could move the antenna in different

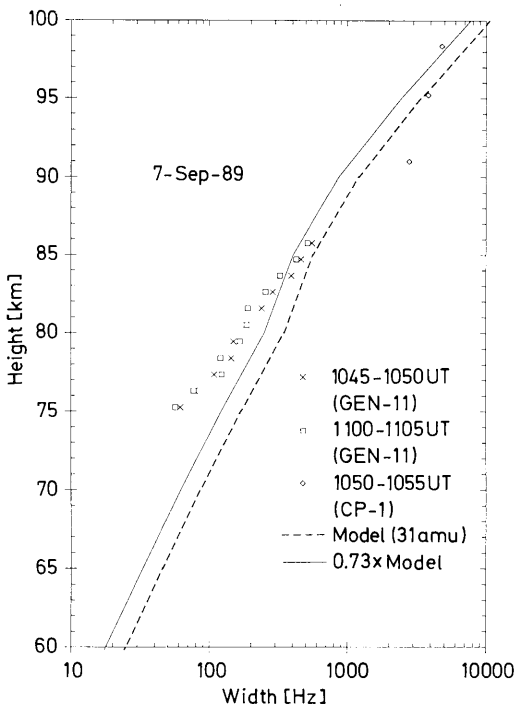

Fig. 8. Variation of spectral width over an extended height range using the multi-pulse technique (CP-1) above 90 km, and the pulse-to-pulse technique (GEN-11) below 90 km. The narrowing of spectral width below 85 km suggests an increase of positive ion mass

directions to obtain both the meridional and zonal winds. Such schemes should be implemented during future measurements during PCAs using EISCAT.

Spectral width results

In Fig. 7, we present profiles of spectral width from a number of experiments: 1. four during PCA conditions, the same as shown in Fig. 6; 2. one from 10 March 1989 taken with vertical antenna during the declining phase of a PCA, so the useful altitudes extend down to 75 km; 3. four during non-PCA conditions to provide an idea of the background ionosphere (down to about 70 km), so as to determine whether the results during PCAs have any unusual features. The data from the latter four (6 May 1988, 2 July 1988, 1 July 1985, and 7 September 1989) were obtained under auroral precipitation conditions. We have used the results of the exponential fit to the ACF with the correction factor in Fig. 3b to account for the effects of aliasing. The dashed lines in Fig. 7 are the predicted spectral widths which were also shown in Fig. 4, obtained from Eq. (2) assuming no negative ions, a positive ion mass of 31 amu, and ν_{in} calculated according to Hill and Bowhill (1977) using the mean positive ion and neutral mass density. In the absence of any simultaneous experimental data during these events, we used the neutral density and temperature from the CIRA-86 (70°N) model. As discussed by Hansen *et al.* (1991), the mean positive ion mass below about 85 km may differ significantly from the average value of 31 amu for a 50% NO^+ and 50% O_2^+ gas. Below this altitude, especially in summer when the temperature may be very low, heavy cluster ions may form. Because of the uncertainty in positive ion composition, we do not try to use a complicated model. The effect of heavier ions would be to narrow the expected spectrum, but only up to some limit which is given by Eq. (7) of Hoppe *et al.* (1990). This is because the effect of increasing m_i in Eq. (2) is largely compensated for by a corresponding decrease in ν_{in} according to the model of Hill and Bowhill (1977). In the limit of infinitely heavy ions the spectral width turns out to be 0.73 times that calculated using 31 amu.

It is clear that the data deviate from the expected "CIRA-86" spectral widths quite considerably at times. The solid lines, showing 0.73 times the "CIRA-86" model values, are a better fit to some of the data, especially those taken during PCA's. The non-PCA widths, however, are still around 0.5 times the expected widths. Tepley *et al.* (1981) also found that halving the model spectral widths obtained by using the CIRA-72 model gave better agreement with Arecibo data at heights between 73 and 84 km. That the measured widths above about 70 km are often smaller than the model values has already been reported by Hansen *et al.* (1991) whose Fig. 8 shows all published values of spectral width available to them. Figure 7, together with the results of Tepley *et al.* (1981) and Hansen *et al.* (1991), shows that, although the spectral widths calculated using a heavy positive ion mass are in better agreement with the measured widths in the absence of negative ions than those calculated using 31 amu, there is still an unexplained discrepancy.

In the May data there appears to be a transition from 31 amu to heavier ions just below 80 km, and in the September data a sharper transition just above 82 km. In the data from the PCA events there is no evidence of such a transition, which may be partly due to the sampled heights not exceeding 80 km in most cases. It is expected that the transition from molecular to cluster ions occurs between 80 and 85 km during summer PCA conditions (see Hansen *et al.*, 1991, and their Fig. 3), although there are no measurements from summer PCA events. In general, the effect of enhanced electron density is to move the transition region from molecular to cluster ions downwards by 5–10 km.

During the experiment of 7 September 1989, the D-region experiment was alternated with a more general-purpose experiment (CP-1) which used the multi-pulse technique to measure useful spectra in a ± 16667 Hz bandwidth down to 92.7 km with a 2.7 km height separation. The spectral widths from three heights are plotted in Fig. 8, together with the "GEN-11" data from Fig. 7, which covered the time immediately before and after the multi-pulse modulation. Spectra above the height of 98 km no longer appear Lorentzian and are therefore not plotted. These three multi-pulse data points have a different slope from the lower GEN-11 data but their average value confirms the trend that the model using 31 amu is in better agreement with the data above 85 km than the heavy ion model.

The increase in spectral width below about 70 km in the October and December data (Fig. 7) can be attributed to the effect of negative ions. The electrons can attach to

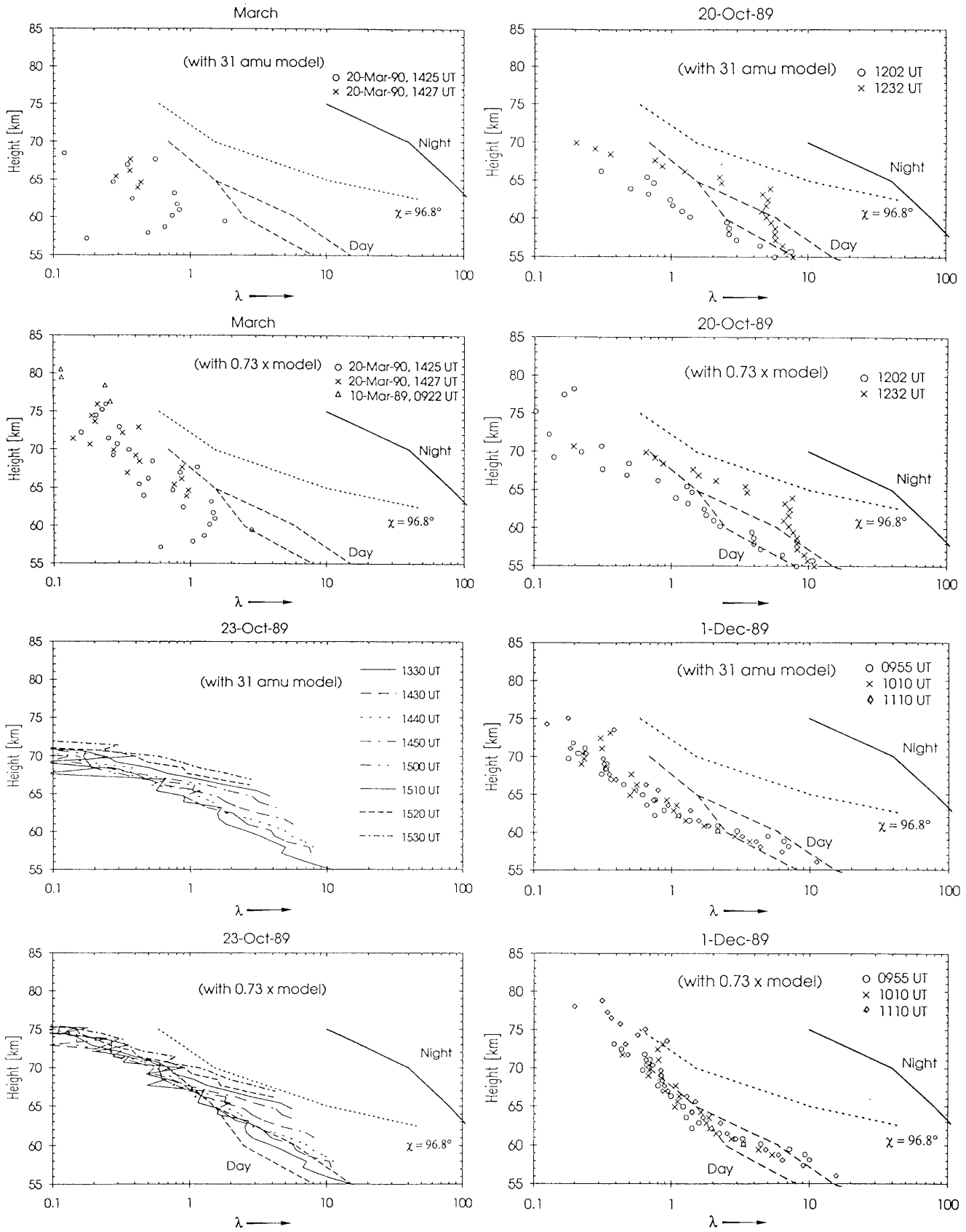

Fig. 9. Negative ion number density to electron number density ratios (λ) deduced using the two theoretical profiles from Fig. 7, for four separate days during PCA conditions. The values in the upper plot in each pair are deduced using the 31 amu model while those in the lower plot are from the heavy ion model. The data from 20 October 1989 are not shown in Fig. 7. The curves show measurements from night (*solid line*), sunset (*dotted line*) and day (*dashed line*) from rocket measurements during a PCA event (Ulwick, 1973)

molecules increasingly easily as sunlight decreases. By using Eq. (2) or (3) the width may be used to estimate λ, assuming that T, ν_{in}, and m_i are known, or in other words, assuming the spectral width in the absence of negative ions is known. We have used the full expression, Eq. (3), which includes the effects of Debye length to calculate λ. The expression for λ becomes:

$$\lambda = (W/W' - 1)(2 + \alpha^2)/2 \quad (5)$$

where W' is given by Eq. (2) and W is the measured width. The top graph of each pair in Fig. 9 shows λ, the negative ion number density to electron number density ratio, derived from the difference between the measured spectral width and the model width using 31 amu, for four of the experiments performed under PCA conditions. The lower graph in each pair shows similar estimates of λ using the CIRA-86 model with heavy positive ion mass. The data above about 75 km for March and 23 October in Fig. 7 are in good agreement with such a model. Even if the absolute values of λ are in error as a result of our model values, relative changes should be only slightly affected. The results from the heavy ion model in Fig. 9 are more consistent with what one would expect based on previous measurements (e.g. Ulwick, 1973). Our data are mainly from daytime or sunset ionospheres, which probably explains the small values we obtain for λ down to 70 km compared with other published results which were obtained mainly at night (Hall and Brekke, 1988; Hall *et al.*, 1988). We note that Hansen *et al.* (1991) also reported small (<1) values down to 70 km for their daytime data during the August PCA. Furthermore, most previous EISCAT results have been obtained with VHF radar data (except Hall *et al.* (1988), and Hansen *et al.* (1991)) and so far no systematic comparison between simultaneous D-region results from the UHF and VHF radars has been done.

In Fig. 17 of Collis and Rietveld (1990), we presented another estimate of λ for 23 October 1989, using the difference between the daytime and night-time electron densities, which gives larger values than those presented here and which were consistent with previous night-time estimates obtained by Ulwick (1973). Those larger values should be representative of the night-time negative ion ratios whereas those presented here are appropriate for sunset.

The data for 23 October 1989 in Fig. 9c clearly shows how, at a given altitude, the negative ion ratio increases with time or solar zenith angle, until the returned power (from the electrons) becomes too weak to make a valid measurement possible. Figure 10 shows how λ varies as a function of time at height intervals of approximately 2 km during sunset. The time resolution is 2 min, and, even if there is some doubt concerning the absolute values of λ because of the uncertainty in the model background ionosphere, the relative increases as a function of time should be correct. A detailed comparison of the time of initial increase in λ from Fig. 10 with the time of initial decrease in electron density from Fig. 14 of Collis and Rietveld (1990) shows very close agreement, reinforcing the interpretation of free electrons being removed by attachment to molecules. As a further check of consistency, we calculated the total positive ion density as a function of time at various heights by multiplying the electron density by $(1+\lambda)$. Now since the backscattered power depends on λ as given by Eq. (4) of Hoppe *et al.* (1990) for example, the electron density was calculated in a self-consistent manner from the backscattered power by initially assuming no negative ions, then calculating λ_D and λ, then recalculating the density using the new values of λ_D and λ, and repeating this procedure a few times to convergence. The result of the calculation showed that the positive ion density remained constant throughout sunset to within a few tens of percent, whereas the electron density decreased by much more, e.g. a factor of 3 at 66 km (Fig. 8b of Collis and Rietveld, 1990). That the positive ion density should remain constant below 70 km is to be expected if the ionising proton flux remains relatively constant over this brief interval, as it did according to GOES-7 satellite data (Fig. 5 of Collis and Rietveld, 1990).

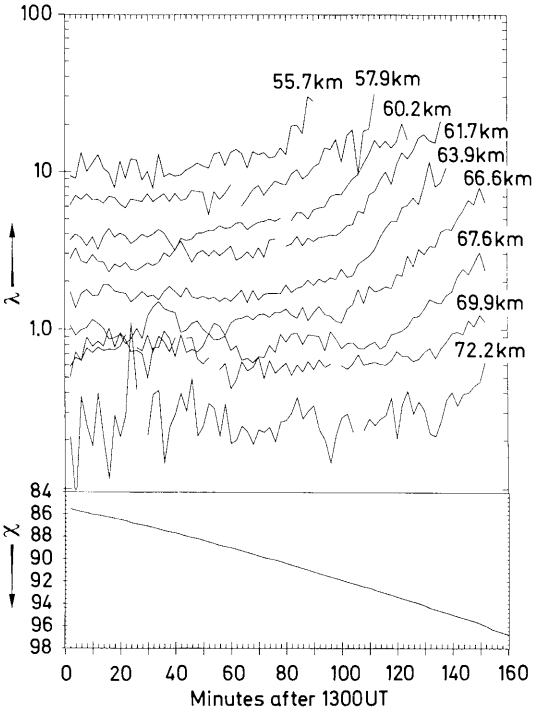

Fig. 10. Variation of λ (upper panel) with time (2-min resolution) at various heights in 2-km intervals during sunset on 23 October 1989. Gaps are caused by poor fits to the measured spectra. The background ionosphere is assumed to be represented by the model values from Fig. 7 with a heavy positive ion mass. The lower panel shows the solar zenith angle (χ)

An additional point to consider in interpreting the observations is that the spectral width calculated from Eq. (2) assumes T_e/T_i to be equal to one. Hansen *et al.* (1991) commented that T_e/T_i would need to be larger than five to explain the discrepancy in the spectral widths, which was considered unrealistic in the D-region. One factor which was not considered is possible self-heating of the electrons in the D-region by the powerful radar probing pulses themselves. The only published results of self-heating were by Coco and Ganguly (1982) who reported a T_e/T_i of about two from 208 μs, 430 MHz pulses from the Arecibo radar in the height region 65–75 km. At our

radar frequency of 933 MHz the Ohmic heating effect should be smaller than at 430 MHz, but the electron densities, and possibly the electron-neutral collision frequencies during these PCA conditions are undoubtedly higher than the Arecibo values, increasing the effect of heating. Calculations by Rietveld and Stubbe (1987) of the self-heating effect for the full-power 5 MW VHF (224 MHz) radar suggested that T_e/T_i may exceed three at 50–60 km, but smaller values would be reached above 70 km. It would appear therefore unlikely that self-heating can completely explain the discrepancies, even if it does contribute to them.

Conclusion

ISR spectral measurements at 933 MHz were obtained down to 55 km altitude during three separate PCA events in 1989–1990. Two approaches were tested in deriving parameters from the spectral data. Fitting an exponential to the ACFs was found to give the most reliable spectral widths, especially for larger values, compared to fitting a Lorentzian curve to the spectrum. The mean Doppler shift enabled meridional wind profiles to be measured, showing long period (>6 h) wave-like variations. Longer data series are required if such long period waves are to be studied in detail in the future.

The spectral widths above about 70 km altitude were often found to be narrower than model values based on the CIRA-86 model and an assumed positive ion mass of 31 amu, which confirms the results of other work (Hansen *et al.*, 1991). This discrepancy may be partly caused by inaccurate knowledge of positive ion mass, temperature and atmospheric density, or possibly through a self-heating effect of the radar pulse on the electrons.

Below 70 km, the observed broadening of the spectral width can be attributed to the formation of negative ions, especially after sunset. Calculated negative ion number density to electron number density ratios (λ) are consistent with values measured using rockets if we assume a very heavy positive ion mass instead of 31 amu. Daytime values of λ varied from about 0.3 at 72 km to about 10 at 55 km. A transition through sunset enabled the increase in λ to be measured as a function of time in altitude steps of a few km. However, because of the unexplained discrepancy between model and measured spectral widths at the upper altitudes where we expect the effect of negative ions to be small, the deduced absolute values of λ, especially at the lower altitudes, must be regarded with some caution.

In future EISCAT measurements during PCA events, combined VHF and UHF data may help resolve some of the remaining questions such as the effect of self-heating on the spectra. Indeed, a brief period of simultaneous artificial HF heating of the electrons at very low altitudes during a PCA event using the heating facility may confirm and calibrate the expected narrowing of spectral width as T_e/T_i is increased. Combined UHF and VHF radar measurements could also be used to measure meridional and zonal winds simultaneously. Use of the VHF radar should extend these measurements to lower densities and heights compared to the UHF radar alone.

Acknowledgements. We thank the EISCAT staff for the radar operation during these unusual events. The EISCAT Scientific Association is supported by the Centre National de la Recherche Scientifique of France, Suomen Akatemia of Finland, Max-Planck-Gesellschaft of Germany, Norges Almenvitenskaplige Forskningsråd of Norway, Naturvetenskapliga Forskningsrådet of Sweden, and the Science and Engineering Research Council of the United Kingdom.

References

Balsley, B. B., W. L. Ecklund, and D. C. Fritts, VHF echoes from the high-latitude mesosphere and lower thermosphere: Observations and interpretations, *J. Atmos. Sci.*, **40,** 2451, 1983.

Coco, D., and S. Ganguly, Heating at 430 MHz in the lower ionosphere at Arecibo, *J. Geophys. Res.*, **87,** 7551–7556, 1982.

Collis, P. N., and M. T. Rietveld, Mesospheric observations with the EISCAT UHF radar during polar cap absorption events: 1. Electron densities and negative ions, *Ann. Geophys.*, **8,** 12, 809–824, 1990.

Collis, P. N., and J. Röttger, Mesospheric measurements with the EISCAT UHF and VHF radars: a review of principles and experimental results, J. Atmos. Terr. Phys., **52,** 569–584, 1990.

Dougherty, J. P., and D. T. Farley, A theory of incoherent scattering of radio waves by a plasma 3. Scattering in a partially ionized gas, *J. Geophys. Res.*, **68,** 5473–5486, 1963.

Fukuyama, K., and W. Kofman, Incoherent scattering of an electromagnetic wave in the mesosphere: a theoretical consideration, *J. Geomagn. Geoelectr.*, **32,** 67–81, 1980.

Fukuyama, K., Y. Maekawa, S. Fukao, and S. Kato, Ionospheric D-region temperatures, and electron and neutral densities observed by the incoherent scatter technique at Arecibo, *Ann. Geophys.*, **5,** 289–296, 1987.

German, M. J., and J. D. Mathews, Interference detection and correction applied to incoherent scatter power profile measurements, *Radio Sci.*, **21,** 745–751, 1986.

Hall, C., and A. Brekke, High Schmidt numbers in the mesopause region from 224 MHz incoherent backscatter, *Geophys. Res. Lett.*, **15,** 561–564, 1988.

Hall, C., T. Devlin, A. Brekke, and J. K. Hargreaves, Negative ion to electron number density ratios from EISCAT mesospheric spectra, *Phys. Scripta*, **37,** 413–418, 1988.

Hansen, G., U. P. Hoppe, E. Turunen, and P. Pollari, Comparison of observed and calculated incoherent scatter spectra from the D-region, *Radio Sci.*, **26,** 1153–1164, 1991.

Hill, R. J., and S. A. Bowhill, Collision frequencies for use in the continuum momentum equations applied to the lower ionosphere, *J. Atmos. Terr. Phys.*, **39,** 803–811, 1977.

Hoppe, U. P., and T. L. Hansen, Studies of vertical motions in the upper mesosphere using the EISCAT UHF radar, *Ann. Geophys.*, **6,** 181–185, 1988.

Hoppe, U. P., D. C. Fritts, I. M. Reid, P. Czechowsky, C. M. Hall, and T. L. Hansen, Multiple-frequency studies of the high-latitude summer mesosphere: implications for scattering processes, *J. Atmos. Terr. Phys.*, **52,** 907–926, 1990.

Kofman, W., A mesospheric experiment: measurement scheme and program implementation, *EISCAT Tech. Note 82/35,* EISCAT Scientific Association, Box 812, S-981 28 Kiruna-Sweden, 1982.

Mathews, J. D., The effect of negative ions on collision-dominated Thomson scattering, *J. Geophys. Res.*, **83,** 505–512, 1978.

Mathews, J. D., The incoherent scatter radar as a tool for studying the ionospheric D-region, *J. Atmos. Terr. Phys.*, **46,** 975–986, 1984.

Mathews, J. D., Incoherent scatter radar probing of the 60–100-km atmosphere and ionosphere, *I.E.E.E. Trans. Geosci. Remote Sensing*, **GE-24,** 765–776, 1986.

Pollari, P., A. Huuskonen, E. Turunen, and T. Turunen, Range ambiguity effects in a phase-coded D-region incoherent scatter radar experiment, *J. Atmos. Terr. Phys.*, **51,** 937–945, 1989.

Reagan, J. B., and T. M. Watt, Simultaneous satellite and radar studies of the D-region ionosphere during the intense solar particle events of August 1972, *J. Geophys. Res.*, **81,** 4579–4596, 1976.

Rees, D., COSPAR International Reference Atmosphere: 1986 Part II: Middle Atmosphere Models, *Adv. Space Res.*, **10,** 12, 1990.

Rietveld, M. T., and P. Stubbe, Ionospheric demodulation of powerful pulsed ratio waves: A potential new diagnostic for radars suggested by Tromsø heater results, *Radio Sci.*, **22,** 1084–1090, 1987.

Röttger, J., and W. Meyer, Tidal wind observations with incoherent scatter radar and meteorological rockets during MAP/WINE, J. Atmos. Terr. Phys., **49,** 689–703, 1987.

Rüster, R., P. Czechowsky, and G. Schmidt, VHF radar observations of tides at polar latitudes in the summer mesosphere, *J. Atmos. Terr. Phys.*, **12,** 1041–1046, 1988.

Tepley, C. A., J. D. Mathews, and S. Ganguly, Incoherent scatter radar studies of mesospheric temperatures and collision frequencies at Arecibo, *J. Geophys. Res.*, **86,** 11330–11334, 1981.

Tsuda, T., S. Kato, T. Yokoi, T. Inoue, M. Yamamoto, T. E. VanZandt, S. Fukao, and T. Sato, Gravity waves in the mesosphere observed with the middle and upper atmosphere radar, *Radio Sci.*, **26,** 1005–1018, 1990.

Turunen, T., GEN-SYSTEM – a new experimental philosophy for EISCAT radars, *J. Atmos. Terr. Phys.*, **48,** 777–785, 1986.

Turunen, E., P. N. Collis, and T. Turunen, Incoherent scatter spectral measurements of the summertime high-latitude D-region with the EISCAT UHF radar, J. Atmos. Terr. Phys., **50,** 289–299, 1988.

Ulwick, J. C., Steady state coefficients in the D-region during solar particle events, *Space Res.*, **XIII,** 581–586, 1973.

Wisemberg, J., and G. Kockarts, A new ionospheric scattering mechanism, *J. Atmos. Terr. Phys.*, **45,** 47–53, 1983.

Ying, W. P., J. D. Mathews, and P. K. Rastogi, Interference detection and correction applied to D region incoherent scatter power spectral measurements, *Radio Sci.*, **22,** 307–312, 1987.